COMMUNICATION

PCCP
www.rsc.org/pccp

Collective ionic motion in oxide fast-ion-conductors

Chris E. Mohn,[a] Neil L. Allan,[b] Colin L. Freeman,[b] Ponniah Ravindran[a] and Svein Stølen*[a]

[a] *Department of Chemistry, University of Oslo, Postbox 1033, Blindern, N0315 Oslo, Norway. E-mail: svein.stolen@kjemi.uio.no*
[b] *University of Bristol, School of Chemistry, Cantock's Close, Bristol, UK, BS8 1TS*

Received 2nd April 2004, Accepted 6th May 2004
First published as an Advance Article on the web 12th May 2004

Structural correlations and dynamic disorder in the oxide fast-ion-conductor $Ba_2In_2O_5$ are deduced from a systematic study of the energy-hypersurface using periodic density-functional theory examining 2×10^4 local energy minima. The structure observed experimentally is interpreted as a time and spatial average of those minima which are energetically-accessible. The nature of these has extensive implications for the ionic conductivity. Transition paths connecting minima, characterized using the nudge-elastic-band method, indicate that low-energy collective ion movements must play important rôles in oxide fast-ion conductors such as $Ba_2In_2O_5$. Saddle-points energies for collective transport are lower in energy than those for conventional single-jump mechanisms.

The complexity of grossly disordered structures hinders fundamental understanding of the functional properties of many classes of advanced materials. Links between the dynamic structure, thermodynamic behaviour and ionic and electronic conductivity are central themes in contemporary solid-state science and disordered materials remain a challenge both to experiment and theory. The present contribution focuses on fast-ionic conduction, using $Ba_2In_2O_5$ as a model system. $Ba_2In_2O_5$ exhibits a discontinuous jump in the ionic conductivity of more than one order of magnitude at 1173 K giving an ionic conductivity equal in magnitude to that of the widely used stabilized zirconias.[1] The increase in conductivity is attributed to an order–disorder transition involving oxygen atoms and vacancies. The structural aspects of the disordering and how this relates to the mechanism of ionic conductivity are of intense interest. Present models most often describe the structures and thermodynamics of this and related materials in terms of random distributions of oxygen atoms and oxygen vacancies on the available oxygen sites and their dynamic behaviour in terms of single or correlated ion-jump mechanisms.[2] The purpose of this letter is to present a new, different model for grossly non-stoichiometric oxides in which significant vacancy–vacancy interactions strongly influence the local structural environment and to discuss the implications for the ionic conductivity.

The generic brownmillerite crystal structure $A_2B_2O_5$ adopted by $Ba_2In_2O_5$ consists of alternating two-dimensional layers of cooperatively tilted BO_6 octahedra and ordered arrangements of BO_4 tetrahedra. There are three crystallographically distinct oxygen sites: O(1) in the equatorial plane of the octahedra, O(2) at the apices of the octahedra and O(3) those oxygens in the tetrahedra which are not shared with the octahedra. We investigate the structural features of $Ba_2In_2O_5$ at high temperatures through a thorough study of the full energy hypersurface of a $2 \times 2 \times 2$ cell containing 36 atoms constructed by doubling a primitive cubic unit cell along each of the crystallographic directions. All possible arrangements of the oxygen vacancies are considered. Initially 20 oxygen atoms are distributed over the 24 oxygen lattice sites of the ABO_3 supercell (giving 10626 *initial unrelaxed* arrangements). A symmetry routine reduces this total to 78 *initial unrelaxed* crystallographically non-equivalent arrangements. Structural optimizations (with respect to *all* unit cell dimensions and atomic coordinates) of each arrangement are performed within periodic density functional theory (DFT) and the generalized gradient approximation (GGA) using a sufficiently large basis of projected augmented plane waves (a constant energy cut-off of 700 eV), as implemented in the Vienna *ab initio* simulation program (VASP).[3,4] The optimizations are accompanied by large structural changes. Inspection of the optimized configurations guides our approach for finding additional local energy minima. At this stage other possible crystallographic sites (eight additional active sites for O(3)) within the initial cell are considered. A final total of 81 *relaxed* crystallographic non-equivalent configurations (CNCs) are thus obtained which, using the symmetry routine to determine the degeneracy of each CNC, gives a total of 21 500 *relaxed* local energy minima configurations. We stress the importance of full structural optimizations of the configurations. These are crucial since large energy changes accompany the structural relaxations and these determine not only the magnitude of the energy differences between the CNCs but even the relative order of energies.

The final energy *vs.* degeneracy plot for the $2 \times 2 \times 2$ cell is given in Fig. 1, where each symbol refers to a separate *relaxed* crystallographic non-equivalent configuration. The numbers given in brackets for some CNCs represent the number of indium atoms with 2, 3, 4, 5 and 6 oxygen nearest neighbours, *e.g.* (00404) denotes four four-coordinate In-atoms and four six-coordinate In-atoms in the cell. Our choice of supercell does not permit formation of the stacking of tetrahedral layers observed experimentally in the ordered low-temperature form[5,6] (see structure marked C in Fig. 1). The energy of this structure is calculated from an orthorhombic 18-atom cell and shown by a blue star in Fig. 1. Several of the lowest-energy CNCs contain 50% octahedra and 50% tetrahedra (as indicated by red stars) and resemble the brownmillerite-type structure in that their structures consist of alternate layers of InO_4-tetrahedra and InO_6-octahedra. In the lowest energy CNC for the $2 \times 2 \times 2$ cell, the tetrahedra are linked to form chains (see the chains in blue below the graph in Fig. 1) as in the low-temperature form[5,6] but the stacking from one tetrahedral layer to the next differs as illustrated in the lower part of Fig. 1 (compare structures marked C and B). Other types of connectivities within the tetrahedral layers are also observed. The zig-zag arrangement marked A in Fig. 1 represents one type of connectivity whereas others involves edge-sharing tetrahedra. Although we are using a $2 \times 2 \times 2$ super cell and only see a limited range of the low energy configurations the calculations relate well to the different types of disorder

DOI: 10.1039/b405013d

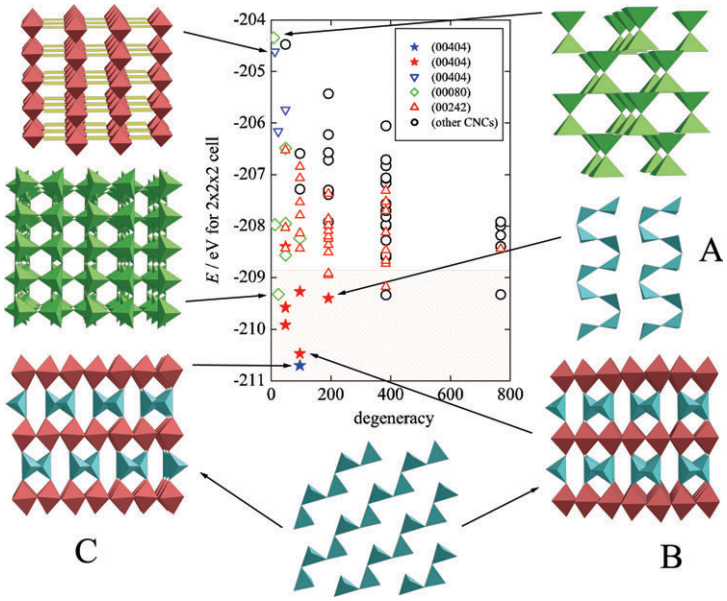

Fig. 1 Energy-degeneracy plot for a 2 × 2 × 2 cell of $Ba_2In_2O_5$. Numbers in brackets show number of In-atoms with 2, 3, 4, 5 or 6 surrounding oxygen atoms (the total number of In-atoms is 8). The (00404) CNCs marked by red stars contain InO_4-tetrahedra and blue triangles denote CNCs containing InO_4 square-planar entities. The energy of the experimentally observed structure is calculated from an orthorhombic 18-atom cell and shown by a blue star. Polyhedral representations of selected CNCs are also included in the figure. Octahedra are red, square pyramids green, tetrahedra blue and square planar entities yellow. For the low-energy (00404) configurations also the connectivity in the tetrahedral layers is shown. The red dashed area identifies the energy region populated significantly at 2500 K (see text).

observed in brownmillerite-structured compounds by transmission electron microscopy.[7–9] In our interpretation, these reflect quenched-in higher-temperature dynamic disorder.

The CNC closest in energy to these low energy (00404)s is a (00080) (given by green symbols in Fig. 1). In all (00080)s one oxygen ion is removed from each InO_6-octahedron yielding structures built up from corner-sharing square pyramids and the lowest energy (00080)-CNC resembles the ordered structure adopted by related compounds such as $Sr_2Mn_2O_5$.[10] Other low energy configurations contain mixtures of tetrahedra, square pyramids and octahedra.

Our detailed systematic search of the potential energy hypersurface also allows us to consider the properties of higher energy CNCs. For example, the highest-energy (00404), marked by a blue triangle in Fig. 1, is closely related to the structure observed for $La_2Ni_2O_5$.[11] In this and other high energy (00404)s, unlike the low-energy (00404)s, the four-coordinate geometry involves a square planar entity which for $Ba_2In_2O_5$ is much less favourable than tetrahedral. This feature is very important for ion transport and will be discussed further below.

The configurations which are energetically accessible at a given temperature can be thought of as representing snapshots of small regions of the disordered materials; the calculations thus identify local structural environments and structural correlations. This is in accordance with the observation of short-length-scale non-cubic micro-domains in NMR experiments[12] and the average structure observed experimentally can be interpreted as a time and spatial average of the different local environments. The fractions of the different polyhedra as a function of temperature, are plotted in Fig. 2a. These are obtained by evaluating the appropriate thermodynamic (Boltzmann) average over all the configurations studied.[13,14] Vibrational contributions to the Gibbs energy of each configuration are ignored. The fractions of octahedra and tetrahedra both remain close to 0.5 up to 2100 K. On increasing the temperature further, the number of square pyramids increases giving a smaller number of tetrahedra and octahedra. The high-energy

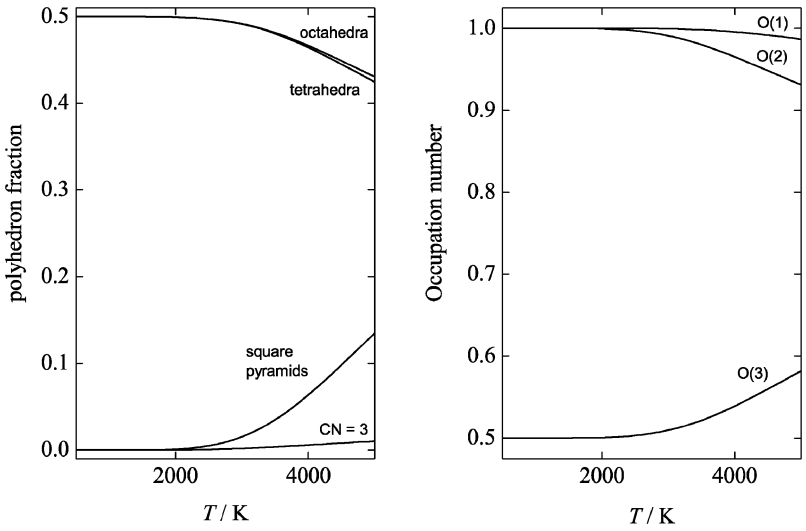

Fig. 2 (a) Fraction of polyhedra and (b) occupancy of the three oxygen sites as a function of temperature.

configurations contribute to thermodynamic properties only to a very limited degree even at high temperatures. The red dashed area of Fig. 1 shows the CNCs that contribute significantly at 2500 K; all other CNCs together contribute about 0.2%. Although the overall fractions of the various polyhedra remain almost constant up to 2100 K, the disorder arising from different arrangements of these polyhedra and thus the configurational entropy are significant even at lower temperatures. Our results are in line with the entropy of the disordered phase being considerably lower than the ideal value obtained by the usual assumption that the oxygen atoms and vacancies are distributed randomly on the oxygen sub-lattice of the perovskite-type structure.[15,16] The reduced entropy is due the small number of energetically accessible configurations at the temperatures considered here.

The energies of the different local structural environments give valuable information that must be taken into account when considering mechanisms of ion transport. A conventional vacancy jump mechanism requires different types of local short-range order that we show here are high in energy and thus make a negligible contribution. The ionic movement is highly restricted by the local symmetry as seen e.g. by the high energy of the square-planar relative to the tetrahedral entity. The occupancy of the O(1), O(2) and O(3) sites shown in Fig. 2b completes the picture. O(1) and O(2) are fully populated up to 2100 K after which the population of O(2) decreases significantly. O(1) is fully populated even at significantly higher temperatures which supports the two-dimensional disorder and conductivity at intermediate temperatures reported previously.[12]

Furthermore, the nature of the low-energy structural configurations has extensive implications for the ionic conductivity. We have investigated transition paths connecting low-energy CNCs using the climbing image nudged-elastic-band method.[17,18] A set of *initial* configurations representing a discrete path between two local minima configurations is constructed using some (usually linear) interpolation. Neighbouring configurations are connected with spring forces. A constrained minimisation of the total energy (including both true interaction energy and unphysical spring energies) is carried out in which the parallel component of the true interaction force and the perpendicular component of the net spring force are projected out. The results indicate strongly that collective ion movements are important in fast oxide-ion conductors such as $Ba_2In_2O_5$.

We use the minimum energy path connecting the (00404)-CNC with a zig-zag pattern of tetrahedra (marked A in both Figs. 1 and 3) and the (00404)-CNC with chains of tetrahedra (marked B in both in Figs. 1 and 3) as an example to illustrate the collective ionic movement. Structural aspects of the reconstructive transformation are illustrated in Fig. 3 showing the local environment at selected reaction coordinates. The intermediate CNC is structurally similar to A, although here every alternate tetrahedron is considerably distorted compared to A. The energy barrier between these two zig-zag configurations is less than 0.1 eV. The subsequent energy barrier for the formation of B which is crucial for ion transport is only 0.48 eV (for our 36-atom supercell). Using symmetry we can also construct pathways connecting a large number of local energy minima. As an example, a reflection of the path in Fig. 3 through the origin provides a mechanism by which any local energy minimum along the path can be transformed into one which is symmetrically equivalent. Thus, the chain configuration marked B can transform into a mirror-image through a complex pathway passing through three local energy minima. This particular transport mechanism involves O(3)-oxygen sites exclusively in agreement with an earlier NMR-study [12] and the ionic movements thus takes place in the *ab*-plane giving two-dimensional conductivity. Other energy pathways connecting (00404)-CNC's have saddle-points with comparable

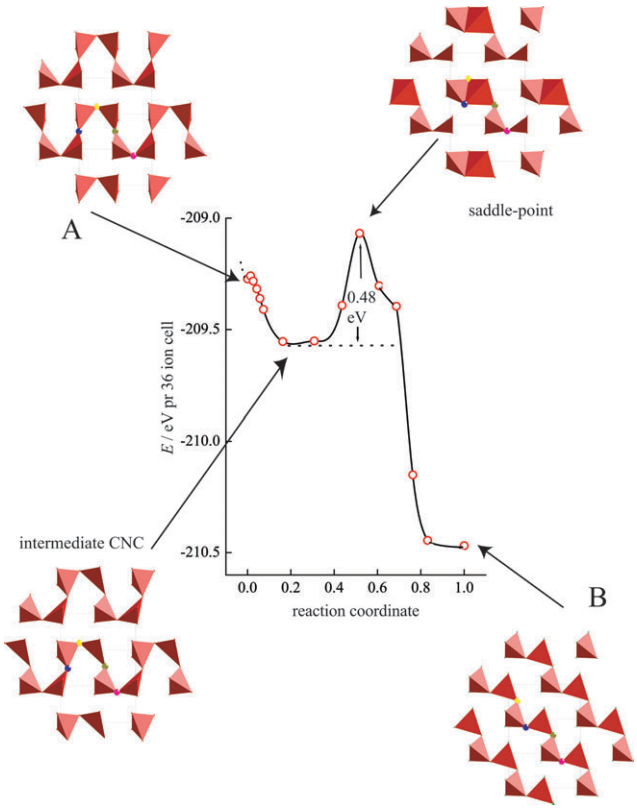

Fig. 3 Minimum energy path connecting the (00404) configurations denoted A and B in Fig. 1. The evolution of the reconstructive transformation is indicated by polyhedron representations of the local environment of selected images as indicated by arrows. The reaction coordinate is defined as the displacement of all ions in the cell from A along the discrete minimum energy path connecting A and B divided by the total displacement of all ions from A to B. The movements of the four oxygen atoms mainly responsible for the chain-transformation can be followed as these are shown using large symbols and different colours. The oxygen atoms marked in blue and yellow undergo the largest displacements and thus contribute most to the oxygen transport.

energy barriers. The energy barrier of the transition path connecting the (00404)-CNC with chains of tetrahedra (marked B in Fig. 3) to the lowest energy (00080), involving motion of both O(3) and O(2) ions, is found to be somewhat higher and so contributes much less to the ion transport.

It is important to stress that the minimum energy pathway gives a saddle-point energy lower in energy than the lowest energy configuration obtained from configuration B in Fig. 1 by moving only one oxygen atom. This shows that collective transport of this kind is energetically significant compared to single-jump mechanisms, the cost of which is high as they involve the breaking of an indium-oxygen bond as the oxygen ion climbs out of its Madelung well. In contrast the collective transport mechanism in $Ba_2In_2O_5$ involves different low-energy local structural environments and simultaneous bond making and bond breaking. In addition to the movement of the oxygen ions giving rise to the transport, other ions are involved and even the Ba- and In-atoms move appreciably in a cooperative fashion along the transition pathway. A larger unit cell will give rise to other types of similar (00404) configurations with different stacking of two or more tetrahedral layers and different connectivities within each tetrahedral layer. The energy barrier for transitions between these will be similar and the cell size does not affect our interpretation of the general features of the transition paths that gives rise to collective ionic motion.

Our approach combining periodic DFT, efficient use of symmetry and transition state location allows us to obtain a unified picture of the link between dynamic structure,

energetics and ion transport in oxide fast-ion conductors such as $Ba_2In_2O_5$. Although the small cell size to which we are restricted by the cost of the first principles calculations approximates the density of states, and thus the temperature scale, our qualitative interpretation of the local order in the disordered state is unaffected. Our method, in which all configurations are explicitly relaxed, differs from the cluster variation method[19] which has proved problematic for perovskites.[20] *Ab initio* molecular dynamics is still unfeasible for these systems due to inaccessible long sampling times. Furthermore, the use of interatomic potentials, needed for classical molecular dynamics, has proved unreliable (unpublished work) mainly due to the large variations in local structure.

The collective ionic motion suggested has similarities to the recent reports of quasi-collective surface diffusion involving several atoms for metal surfaces by transmission electron microscopy[21] and by density-functional theory nudge-elastic-band calculations.[22] In this paper we have identified a collective diffusion mechanism in a bulk ionic material with strong electrostatic interactions. It is tempting to suggest that this type of collective ionic motion is a characteristic of fast ionic conductors in general.

Acknowledgements

This work was funded by Norges Forskningsråd (project number 142995/432). Computational facilities were made available through grants of computer time for the Program for Supercomputing, Norway. CLF is supported by EPSRC grant GR/R85952. Discussions with Truls Norby (UofOslo) and Mikhail Lavrentiev, (UofBristol) are gratefully acknowledged.

References

1 J. B. Goodenough, J. E. Ruiz-Diaz and Y. S. Chen, *Solid State Ionics*, 1990, **40**, 21–31.
2 C. R. A. Catlow, *J. Chem. Soc., Faraday Trans.*, 1990, **86** 1167–1176.
3 G. Kresse and J. Hafner, *Phys. Rev. B*, 1993, **47**, 558–561.
4 G. Kresse and J. Joubert, *Phys. Rev. B*, 1999, **59**, 1758–1775.
5 P. Berastegui, S. Hull, F. J. Garcia-Garcia and S. G. Eriksson, *J. Solid State Chem.*, 2002, **164**, 119–130.
6 S. A. Speakman, J. W. Richardson, B. J. Mitchell and S. T. Misture, *Solid State Ionics*, 2002, **149**, 247–259.
7 M. L. Ruiz-González, C. Prieto, J. Alonso, J. Ramírez-Castellanos and J. M. González-Calbet, *Chem. Mater.*, 2002, **14** 2055–2062.
8 S. Lambert, H. Leligny, D. Grebille, D. Pelloquin and B. Raveau, *Chem. Mater.*, 2002, **14**, 1818–1826.
9 A. M. Abakumov, A. M. Alekseeva, M. G. Rozova, E. V. Antipov, O. I. Lebedev and G. Van Tendeloo, *J. Solid State Chem.*, 2003, **174**, 319–328.
10 V. Caignaert, N. Nguyen, M. Hervieu and B. Raveau, *Mater. Res. Bull.*, 1985, **20**, 479–484.
11 K. Vidyasagar, A. Reller, J. Gopalakrishnan and C. N. R. Rao, *Chem. Commun.*, 1985, 7–8.
12 S. B. Adler, J. A. Reimer, J. Baltisberger and U. Werner, *J. Am. Chem. Soc.*, 1994, **116**, 675–681.
13 N. L. Allan, G. D. Barrera, R. M. Fracchia, M. Yu. Lavrentiev, M. B. Taylor, I. T. Todorov and J. A. Purton, *Phys. Rev. B*, 2001, **63**, 94203.
14 E. Bakken, N. L. Allan, T. H. K. Barron, C. E. Mohn, I. T. Todorov and S. Stølen, *Phys. Chem. Chem. Phys.*, 2003, **5**, 2237–2243.
15 T. R. S. Prasanna and A. Navrotsky, *J. Mater. Res.*, 1993, **8** 1484–1486.
16 T. Hashimoto, Y. Ueda, M. Yoshinaga, K. Komazaki, K. Asaoka and S. R. Wang, *J. Electrochem. Soc.*, 2002, **149**, A1381–A1384.
17 G. Henkelman, B. P. Uberuaga and H. Jonsson, *J. Chem. Phys.*, 2000, **113**, 9901–9904.
18 G. Henkelman and H. Jonsson, *J. Chem. Phys.*, 2000, **113** 9978–9985.
19 J. M. Sanchez, F. Ducastelle and D. Gratias, *Physica A*, 1984, **128**, 334–350.
20 R. McCormack and B. P. Burton, *Comput. Mater. Sci.*, 1997, **8**, 153–160.
21 M. Labayen, C. Ramirez, W. Schattke and O. M. Magnussen, *Nature Mater.*, 2003, **2**, 783–787.
22 G. Henkelman and H. Jonsson, *Phys. Rev. Lett.*, 2003, **90**, 116101.